GDCh Research Article Angewandte International Edition Chemie www.angewandte.org

How to cite: *Angew. Chem. Int. Ed.* **2026**, *65*, e25242
doi.org/10.1002/anie.202525242

Scintillators

Amorphous Zero-Dimensional Organic Metal Halide Hybrid Scintillators with High Light Yield and Fast Response

*Tarannuma Ferdous Manny, Sahel Moslemi, Md Sazedul Islam, Debashis Sen, Ranjan Das, Sulthana Fehroza PP, J. S. Raaj Vellore Winfred, Robert A. Lazenby, Marc Snoeyink, Dennis R. Schaart, and Biwu Ma**

Abstract: Zero-dimensional (0D) organic metal halide hybrids (OMHHs) have recently emerged as a promising class of scintillation materials, offering advantages in performance, tunability, environmental friendliness, and cost-effectiveness. While numerous 0D OMHH scintillators have been developed to date, most of them rely on radioluminescence (RL) originating from metal halide species with long decay lifetimes and are typically prepared as small-sized single crystals via a slow solution growth process. Here, we report for the first time high-performance X-ray scintillators based on facile, solution-processed amorphous 0D OMHH films that exhibit efficient RL with short decay lifetimes enabled by molecular sensitization. By reacting a rationally designed green-emitting organic halide, (4-(9,9-dimethylacridin-10(9*H*)-yl)phenyl)triphenylphosphonium bromide (DMAC-TPPBr), with zinc bromide ($ZnBr_2$), we have obtained amorphous 0D $(DMAC\text{-}TPP)_2ZnBr_4$ films that exhibit outstanding optical and scintillation properties, with a high photoluminescence quantum yield of ~85%, a short photoluminescence decay lifetime (~12.5 ns), a high absolute light yield of ~27,000 photons MeV^{-1}, a radioluminescence decay lifetime of ~8.00 ns, and a low limit of detection (LOD) of ~9.00 nGy_{air} s^{-1}. By leveraging the benefits of solution-processed amorphous OMHHs with molecular sensitization, our approach paves a new pathway toward scalable, low-cost, and fast-response X-ray scintillators.

Introduction

X-ray scintillators, which convert ionizing radiation into visible light, are essential components in modern detection systems and are widely used across diverse fields, including medical imaging, security screening, materials analysis, and high-energy physics.[1–14] Increasingly, applications, particularly dynamic medical imaging modalities such as computed tomography, high-speed angiography, and time-of-flight positron emission tomography, demand scintillators that combine high light yield with ultrafast response. A high light yield enables the detector to capture more photons, producing higher-resolution images at lower radiation doses, while a short decay lifetime minimizes afterglow, preserving spatial sharpness and timing accuracy in fast or real-time imaging environments.[15] Traditional inorganic scintillators like CsI:Tl and Ce:LuAG offer strong X-ray absorption and decent light yields due to their high density and effective atomic number.[16–19] However, their reliance on high-temperature synthesis and complex crystal growth processes leads to high production costs and limits scalability, particularly for flexible or large-area applications. Organic scintillators provide advantages such as mechanical flexibility, low-cost fabrication, and fast response times, but often suffer from low light yields and poor X-ray stopping power due to their low atomic number constituents.[20–22] Recently, metal halide perovskites have attracted significant attention as next-generation materials that bridge the gap between inorganic and organic systems.[23] Their combination of high X-ray absorption, strong luminescence, and solution-processable fabrication makes them highly promising for efficient radiation detection. However, most high-performing perovskite scintillators remain lead-based and crystalline, limiting their flexibility and environmental compatibility.[24,25] Therefore, developing lead-free, amorphous hybrid materials with comparable scintillation efficiency is crucial for enabling flexible, eco-friendly, and large-area X-ray imaging technologies. These challenges underscore the need for next-generation scintillation materials that combine the strengths of both systems, motivating the development of hybrid scintillators with improved performance, processability, and application versatility.

Zero-dimensional (0D) organic metal halide hybrids (OMHHs) have attracted great attention in recent years as promising scintillation materials, particularly following our first report of a 0D organic manganese halide hybrid scintillator in 2020.[1] Since then, tremendous progress has been made in developing 0D OMHH scintillators that

[*] T. F. Manny, S. Moslemi, M. S. Islam, D. Sen, R. Das, S. F. PP, J. S. R. V. Winfred, R. A. Lazenby, B. Ma
Department of Chemistry and Biochemistry, Florida State University, Tallahassee, FL 32306, USA
E-mail: bma@fsu.edu

M. Snoeyink, D. R. Schaart
Department of Radiation Science and Technology, Delft University of Technology, the Netherlands

Additional supporting information can be found online in the Supporting Information section

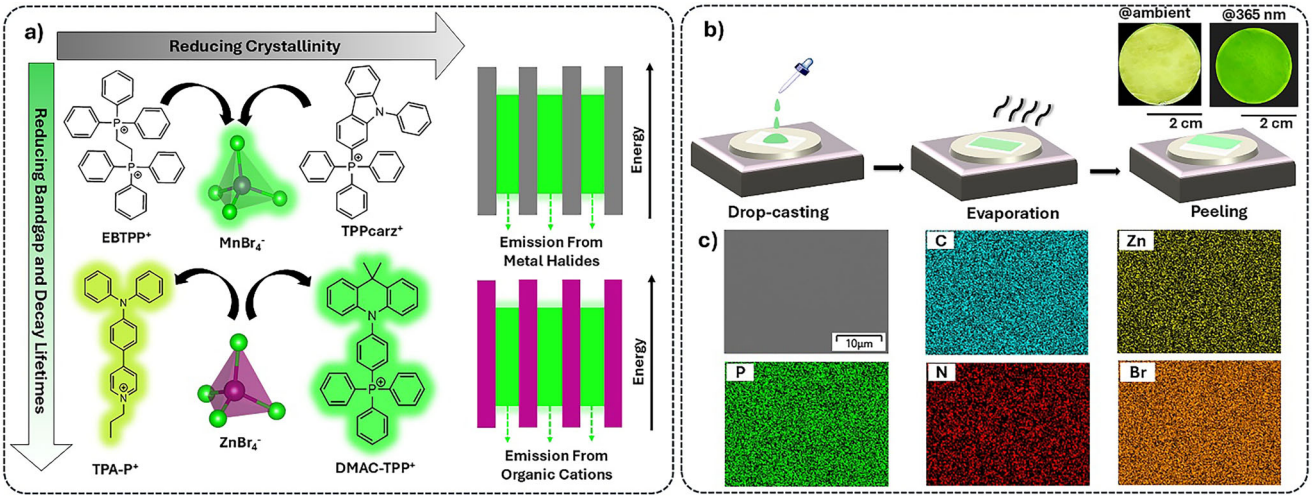

Figure 1. a) Molecular design strategy for developing 0D OMHH scintillators with tunable morphological and photophysical properties, where either the metal halide anions or organic cations serve as emitting centers depending on their bandgaps, and their corresponding energy level diagrams. b) Schematic illustration of the fabrication process for amorphous 0D $(DMAC\text{-}TPP)_2ZnBr_4$ films via solution processing followed by thermal annealing (the inset shows the photographs of a film under ambient and UV (365 nm) illumination). c) Scanning electron microscopy (SEM) image of a 0D $(DMAC\text{-}TPP)_2ZnBr_4$ film along with its elemental mapping of C, Zn,P, N, and Br.

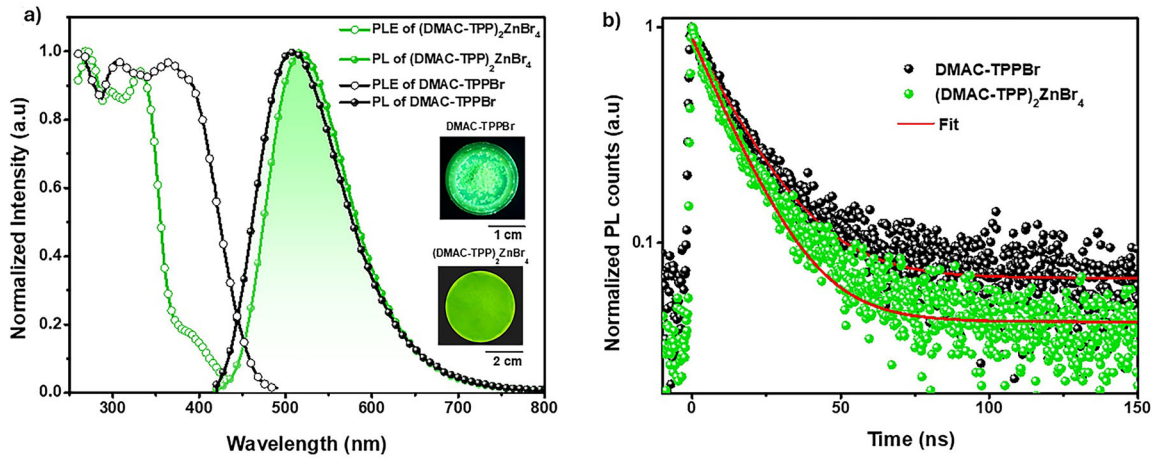

Figure 2. a) Photoluminescence excitation and emission spectra of DMAC-TPPBr and 0D $(DMAC\text{-}TPP)_2ZnBr_4$ (Inset shows the images underUV (365 nm) excitation). The excitation spectra were collected for the emission wavelength at 510 nm and 518 nm for DMAC-TPP and 0D $(DMAC\text{-}TPP)_2ZnBr_4$, respectively. PL spectra were recorded for the excitation wavelength at 365 nm for both compounds. b) Time-resolved photoluminescence of DMAC-TPPBr and 0D $(DMAC\text{-}TPP)_2ZnBr_4$ with mono-exponential decay fitting. Emission decay profiles were recorded for the emission peak at 510 nm and 518 nm for DMAC-TPP and 0D $(DMAC\text{-}TPP)_2ZnBr_4$, respectively.

exhibit high light yields, compositional tunability, and solution processability.[26–34] However, the majority of reported 0D OMHH scintillators rely on radioluminescence (RL) from metal halide centers with long decay lifetimes, typically in the micro- to millisecond range, which limits their suitability for time-resolved detection and high-speed imaging applications.[35–40] Moreover, most are synthesized as small single crystals via slow solution growth methods, posing challenges for scalability and integration into large-area or flexible devices.[28–30,32–34,41] To address the issue of long decay lifetimes associated with metal halide emitting centers, we have developed molecular sensitization enabled single crystalline 0D OMHH scintillators, such as $(TPA\text{-}P)_2ZnBr_4$, in which metal halides act as X-ray sensitizers and organic cations as emitters, achieving decay lifetimes of nanoseconds.[3] To overcome the limitations associated with small-sized 0D OMHH single crystals, there is growing interest in amorphous 0D OMHHs, such as glassy or gel-like films, which can be readily fabricated via facile solution processing followed by mild thermal annealing. These amorphous materials not only eliminate grain boundaries and mechanical brittleness associated with crystalline counterparts but also enable scalable manufacturing.[31,42–49] In our recent work, we demonstrated amorphous 0D OMHH scintillators based on 0D $(TPPcarz)_2MnBr_4$ films with excellent mechanical properties and scalability, although the emission still originates from the metal halide center with long decay lifetimes.[4] To fully unlock the potential of 0D OMHHs for next-generation

fast-response scintillators, a key objective is to develop amorphous 0D OMHHs, in which molecular sensitization enables efficient energy/electron transfer from metal halide X-ray absorbers to organic emitters with high light yields and short RL decay lifetimes.

Here we report for the first time high-performance X-ray scintillators based on solution-processed amorphous 0D OMHHs, in which efficient RL with short decay lifetimes is achieved via molecular sensitization. Our molecular design strategy introduced a highly luminescent organic halide, green-emitting (4-(9,9-dimethylacridin-10(9*H*)-yl)phenyl)triphenylphosphonium bromide (DMAC-TPPBr), and reacted it with zinc bromide ($ZnBr_2$) to obtain amorphous 0D $(DMAC\text{-}TPP)_2ZnBr_4$ films. In this system, the wide-bandgap $ZnBr_4^{2-}$ anions act as X-ray absorbers, while the $DMAC\text{-}TPP^+$ cations serve as efficient light emitters. Structural and morphological analysis confirmed the fully amorphous nature and film uniformity. The resulting films exhibit strong green emission (~518 nm), a high photoluminescence quantum yield (~85%), and a short photoluminescence decay lifetime (~12.5 ns). Under X-ray excitation, the films display a linear, dose-dependent RL response with a fast response (~8.00 ns), a high absolute light yield (~27,000 photons MeV^{-1}), a low limit of detection (9.00 $nGy_{air}\ s^{-1}$), and excellent operational stability. Furthermore, integration onto flexible textile substrates demonstrates their potential for use in wearable and portable X-ray detection devices.

Results and Discussion

Figure 1a illustrates the molecular design strategy for developing 0D OMHH scintillators with high light yields, short decay lifetimes, and enhanced processability. We began with single crystalline ethylenebis-triphenylphosphonium manganese(II) bromide ($(EBTPP)MnBr_4$), a 0D OMHH exhibiting a high light yield of ~80,000 photons MeV^{-1} and luminescence from $MnBr_4^{2-}$ with a long decay lifetime of 318 µs.[1] However, its high crystallinity limits film processability. To overcome this, we introduced noncrystalline $TPPcarz^+$ cations in place of $EBTPP^{2+}$, yielding amorphous 0D $(TPPcarz)_2MnBr_4$.[4] This composition offers improved solution processability and mechanical flexibility, though it retains long-lived metal halide-based RL due to the relatively large bandgap of the $TPPcarz^+$ cation. To achieve shorter decay lifetimes, we adopted a molecular sensitization strategy by pairing a low-bandgap organic cation ($TPA\text{-}P^+$) with a high-bandgap, non-emissive $ZnBr_4^{2-}$ anion. This led to the development of 0D $(TPA\text{-}P)_2ZnBr_4$, which exhibits RL originating from the $TPA\text{-}P^+$ cation with a significantly shortened decay lifetime, although it remains single crystalline.[3] These results point to the promise of continued molecular engineering, particularly through the integration of noncrystalline, low-bandgap emissive organic cations and high-bandgap, non-emissive metal halide anions, to enable amorphous 0D OMHH scintillators with short-lived RL.

In this work, we rationally designed a new amorphous emissive organic halide DMAC-TPPBr to prepare an amorphous 0D OMHH $(DMAC\text{-}TPP)_2ZnBr_4$, exhibiting high light yield and short decay lifetime. Substituting the carbazole unit in $TPPcarz^+$ with a DMAC moiety yielded $DMAC\text{-}TPP^+$ featuring a reduced bandgap while retaining the noncrystalline character. Details of the synthesis and characterization of DMAC-TPPBr are provided in Figures S1–S5 and Table S1. The composition and structure were confirmed by nuclear magnetic resonance (NMR) spectroscopy (Figure S2) and liquid chromatography-mass spectrometry (LC-MS) (Figure S3). The optical bandgap of DMAC-TPPBr was estimated to be ~2.5 eV, based on solid-state absorptance (Figure S4) and cyclic voltammetry measurements (Figure S5 and Table S1). Amorphous 0D $(DMAC\text{-}TPP)_2ZnBr_4$ films could be prepared using a previously established solution-processing method, as illustrated in Figure 1b. Specifically, a 2:1 molar ratio of DMAC-TPPBr and $ZnBr_2$ was dissolved in dimethylformamide (DMF) at room temperature to form a clear, homogeneous solution (~3 M). This solution was drop-cast onto a baking sheet substrate and thermally treated at 100 °C for 24 h. After complete solvent evaporation, a transparent greenish-yellow film was obtained, which could be easily peeled off from the baking sheet. The film thickness could be easily tuned by adjusting the solution concentration and casting area.

To verify the successful formation of amorphous 0D $(DMAC\text{-}TPP)_2ZnBr_4$ films, compositional and structural characterizations were conducted. Figure 1c shows a scanning electron microscopy (SEM) image of a representative film approximately 2 cm in diameter and 1.5 mm thick, along with elemental mapping of C, N, P, Zn, and Br obtained using SEM combined with energy-dispersive X-ray spectroscopy (EDS). The uniform spatial distribution of all elements confirms good compositional homogeneity. The experimentally measured elemental weight percentages closely align with the theoretical values for 0D $(DMAC\text{-}TPP)_2ZnBr_4$ (Figure S6 and Table S2), supporting the formation of the target product with a 2:1 molar ratio of DMAC-TPPBr to $ZnBr_2$. We performed FT-IR to validate the C─H and C─N stretching modes in both DMAC-TPPBr and 0D $(DMAC\text{-}TPP)_2ZnBr_4$ (Figure S9a). To further confirm the presence of zinc bromide, we conducted Raman spectroscopy, as shown in Figure S9b, where the Zn─Br stretching vibration appears at ~190 cm^{-1}.[50] Powder X-ray diffraction (PXRD) was used to evaluate the film's crystallinity. Unlike the sharp diffraction peaks typically seen in crystalline materials, 0D $(DMAC\text{-}TPP)_2ZnBr_4$ films exhibit broad patterns (Figure S7), confirming the film's amorphous structure.[47–49] The thermogravimetric analysis (TGA) and differential scanning calorimetry (DSC) curves (Figure S8) of amorphous 0D $(DMAC\text{-}TPP)_2ZnBr_4$ confirm thermal stability up to ~350 °C, while the DSC curve shows a broad feature indicative of structural relaxation and softening, typical of amorphous solids rather than a defined phase transition of a crystalline compound.[47]

The photophysical properties of DMAC-TPPBr powders and 0D $(DMAC\text{-}TPP)_2ZnBr_4$ films were thoroughly characterized. As shown in Figure 2a, both materials exhibit strong green photoluminescence under 365 nm UV excitation, with emission peaks centered at around 518 nm. The emission of 0D $(DMAC\text{-}TPP)_2ZnBr_4$ is slightly redshifted compared to

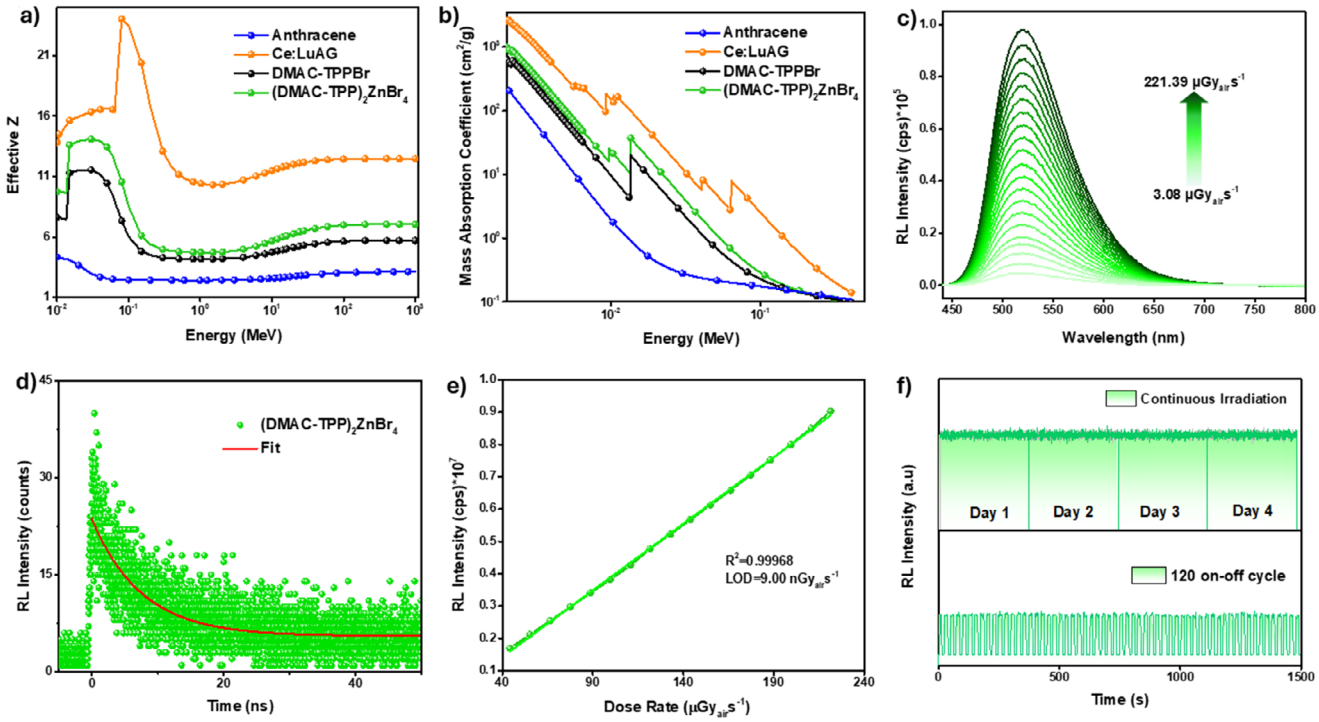

Figure 3. a) Theoretical effective Z values of anthracene, Ce:LuAG, DMAC-TPPBr, and 0D $(DMAC\text{-}TPP)_2ZnBr_4$. b) Theoretical mass absorption coefficients of anthracene, Ce:LuAG, DMAC-TPPBr, and 0D $(DMAC\text{-}TPP)_2ZnBr_4$. c) Dose-dependent RL intensity of 0D $(DMAC\text{-}TPP)_2ZnBr_4$. d) RL decay profile of 0D $(DMAC\text{-}TPP)_2ZnBr_4$. e) The dependence of RL on the radiation dose rate for 0D $(DMAC\text{-}TPP)_2ZnBr_4$. f) Stability of 0D $(DMAC\text{-}TPP)_2ZnBr_4$ under continuous irradiation of X-rays for several days and on-off cycles.

that of DMAC-TPPBr, likely due to more compact molecular packing in the hybrid structure. The photoluminescence quantum yields (PLQYs) were measured to be approximately 79% (Figure S10a) for DMAC-TPPBr and 85% for 0D $(DMAC\text{-}TPP)_2ZnBr_4$ (Figure S10b), respectively. The photoluminescence excitation (PLE) spectra show close similarity for both materials. Importantly, $(DMAC\text{-}TPP)_2ZnBr_4$ films retained a PLQY of 82.3% after 8 months of ambient storage, corresponding to nearly 97% of the original 85% value, demonstrating excellent long-term stability (Figure S10c). To gain further insight into the excited-state dynamics, time-resolved photoluminescence (TRPL) measurements were performed. As shown in Figure 2b, both samples exhibit mono-exponential decay behavior, with lifetimes of 15.7 ns for DMAC-TPPBr and 12.5 ns for $(DMAC\text{-}TPP)_2ZnBr_4$, respectively. The close similarity in emission spectra and decay lifetimes suggests that the luminescence in both materials originates from the same emissive species, the $DMAC\text{-}TPP^+$ cation, which exhibits intramolecular charge transfer (ICT) characteristics supported by transient absorption spectra (Figure S11).[3] The replacement of Br^- by $ZnBr_4^{2-}$ enhances the molecular packing of $(DMAC\text{-}TPP)_2ZnBr_4$ with enhanced radiative decay and higher PLQY, while leaving the emission from $DMAC\text{-}TPP^+$ cations unchanged.

To evaluate the X-ray scintillation potential of the developed materials, we first calculated their mass absorption coefficients and effective atomic numbers (Z_{eff}) and then compared them with those of the standard organic scintillator anthracene and the inorganic scintillator Ce:LuAG to assess their X-ray attenuation capabilities. The energy-dependent effective atomic number (Z_{eff}) was calculated using software developed by Taylor et al.[51] As shown in Figure 3a, 0D $(DMAC\text{-}TPP)_2ZnBr_4$ exhibits a higher effective Z in the photoelectric absorption region (<1 MeV), more than standard anthracene, further confirming its superior X-ray absorption potential. Based on data from the National Institute of Standards and Technology (NIST),[52] the mass absorption coefficients of DMAC-TPPBr and 0D $(DMAC\text{-}TPP)_2ZnBr_4$ were determined. As shown in Figure 3b, both materials display similar absorption at low photon energies (~1 keV). However, at higher photon energies, 0D $(DMAC\text{-}TPP)_2ZnBr_4$ exhibits significantly higher absorption than DMAC-TPPBr, attributed to the presence of zinc, which enhances X-ray attenuation. In addition, the X-ray absorption coefficients of the standard organic scintillator polyvinyltoluene (PVT) and $(DMAC\text{-}TPP)_2ZnBr_4$ were compared as a function of photon energy (Figure S12a), showing that $(DMAC\text{-}TPP)_2ZnBr_4$ exhibits much higher absorption in the low-energy region due to the presence of heavier Zn and Br atoms that enhance photoelectric interactions. The attenuation efficiency as a function of material thickness (Figure S12b) further demonstrates that $(DMAC\text{-}TPP)_2ZnBr_4$ achieves over 90% attenuation within 1 mm, whereas PVT remains significantly less efficient. Together, these results highlight the superior X-ray stopping power of $(DMAC\text{-}TPP)_2ZnBr_4$ compared to conventional organic scintillators, confirming its strong potential as a high-performance

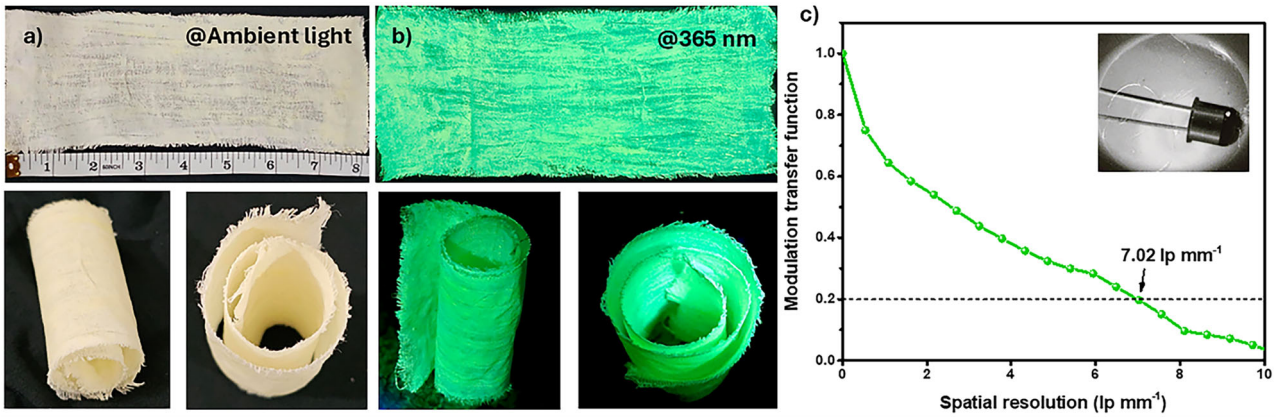

Figure 4. a) A wearable scintillating fabric containing 0D $(DMAC\text{-}TPP)_2ZnBr_4$ under ambient light. b) A wearable scintillating fabric containing 0D $(DMAC\text{-}TPP)_2ZnBr_4$ under UV(365 nm) light. c) Modulation transfer function (MTF) curve of the scintillating fabric obtained using the slanted-edge method, showing a spatial resolution of 7.02 lp mm^{-1}.

material for efficient X-ray detection. This improvement positions 0D $(DMAC\text{-}TPP)_2ZnBr_4$ as a more promising candidate for certain scintillator applications. Distinct K-edge absorption features are observed in the absorption spectra, i.e., DMAC-TPPBr shows two edges corresponding to phosphorus and bromine, while 0D $(DMAC\text{-}TPP)_2ZnBr_4$ exhibits an additional edge due to the presence of zinc.

The RL properties of amorphous 0D $(DMAC\text{-}TPP)_2ZnBr_4$ films were evaluated under X-ray irradiation. An X-ray generator (Moxtek Mini tube, W target, 4 W) coupled with Edinburgh FS5 fluorescence spectrophotometer was used for RL measurements. As shown in Figure 3c, the films emit bright green light peaking at 518 nm under ~10.3 keV X-ray irradiation, consistent with their photoluminescence (PL) under 365 nm UV excitation. The RL intensity of 0D $(DMAC\text{-}TPP)_2ZnBr_4$ exhibits excellent linearity with respect to X-ray dose rate over a broad range (Figure 3c). Light yield, a key performance metric for scintillators, was also characterized to evaluate the RL scintillation performance of $(DMAC\text{-}TPP)_2ZnBr_4$. Using the single photoelectron pulse height spectrum measurement method with a ^{241}Am excitation source, the absolute light yield of $(DMAC\text{-}TPP)_2ZnBr_4$ was determined to be ~27,000 photons MeV^{-1} (Figure S13). This outstanding performance surpasses those of commercial inorganic scintillator Ce:LuAG (25,000 photons MeV^{-1}) and organic scintillator anthracene (13,500 photons MeV^{-1}). The RL decay lifetime of $(DMAC\text{-}TPP)_2ZnBr_4$ was measured using a time-correlated single-photon counting technique, with the X-ray tube excited by a PicoQuant LDH-P-C-440 M pulsed diode laser (mean X-ray energy 18.5 keV). As shown in Figure 3d, the RL decay is similar to the PL decay, with a lifetime of ~8.00 ns, much shorter than those of commercial inorganic scintillator Ce:LuAG (70 ns) and organic scintillator anthracene (21.04 ns).[6] The limit of detection (LOD) was determined to be 9.00 nGy_{air} s^{-1} using the 3σ/slope method, well below the minimum dose rate required for medical radiography (5.5 μGy_{air} s^{-1}).[53] The long-term stability of 0D $(DMAC\text{-}TPP)_2ZnBr_4$ films under continuous X-ray exposure was also examined. As shown in Figure 3f, the RL intensity remained stable over 4 consecutive days of irradiation (30 min per day) and over 120 on/off X-ray cycles, demonstrating excellent operational durability. A video showing the RL response under continuous irradiation at a dose rate of 221.39 μGy_{air} s^{-1} is provided in the Supporting Information.

To demonstrate the practical applicability of amorphous 0D $(DMAC\text{-}TPP)_2ZnBr_4$ in flexible scintillators, a wearable scintillating fabric was fabricated using a simple and scalable process. The material was blended with an acrylic binder to form a uniform mixture, which was then applied onto a cotton fabric substrate using a direct painting method. This approach allowed for large-area painting without the need of complex processing or high-temperature treatment. The coated fabric was left to dry under ambient conditions, yielding a flexible, foldable scintillating textile. The resulting fabric retained excellent mechanical flexibility and could be rolled or folded without compromising its luminescent properties. Visually, the coated fabric appears greenish yellow under ambient light and emits bright green light under 365 nm UV excitation, confirming that the photophysical properties of 0D $(DMAC\text{-}TPP)_2ZnBr_4$ are preserved within the fabric matrix. This straightforward fabrication approach highlights the material's potential for integration into wearable scintillator applications.

To validate its functional performance, the scintillating fabric was further evaluated for X-ray imaging using a simple X-ray radiography setup (Figure S14), in which the fabric served as the scintillating detection layer. An opaque plastic capsule containing a metal spring was chosen as the test object. Upon X-ray exposure, the capsule attenuated the radiation, and the scintillating fabric converted the transmitted X-rays into visible light. The resulting radiographic image (Figure S15) clearly revealed the internal metal spring, demonstrating the fabric's ability to enable real-time X-ray imaging through efficient scintillation. To further evaluate the imaging performance of the scintillating fabric, the spatial resolution was measured to be 7.02 lp mm^{-1} using the standard slanted-edge method. The modulation transfer function (MTF) curve (Figure 4c) illustrates how effectively the fabric-based scintillator maintains image contrast across

Table 1: Performance of representative 0D OMHH scintillators developed to date.

Material	Morphological feature	Emitting species	λ_{max} (nm) PL, color	PL decay time (ns)	Light yield (Ph/MeV)	LOD (nGy_{air} s^{-1})	Refs.
$(C_{38}H_{34}P_2)MnBr_4$	Single crystal	$MnBr_4^{2-}$	517 Green	3.18×10^5	80,000	72.8	[1]
$(PPN)_2SbCl_5$	Single crystal	$SbCl_5^{2-}$	635 Orange	4.1×10^3	49,000	191.4	[8]
$(TPA\text{-}P)_2ZnBr_4$	Single crystal	$TPA\text{-}P^+$	550 Green-yellow	3.56	14,700	21.3	[3]
$(TPP\text{-}carz)_2MnBr_4$	Amorphous	$MnBr_4^{2-}$	517 Green	3.92×10^5	44,600	32.42	[4]
$[AEPipz]CuBr_3{\cdot}Br{\cdot}H_2O$	Single crystal	$CuBr_3^{2-}$	500 Bluish-green	1.21×10^5	62,400	95.7	[30]
$[TPPen]_2Mn_{0.9}\ Zn_{0.1}\ Br_4$	Single crystal	$MnBr_4^{2-}$	515 Green	2.96×10^5	68,000	204.1	[37]
$[DADPA]InBr_6H_2O$	Single crystal	$InBr_6^{3-}$	575 Yellow-orange	4.0×10^3	51,875	98.3	[54]
Mn-IG $(C_{20}H_{20}P)_2MnBr_4$	Amorphous	$MnBr_4^{2-}$	520 Green	2.8×10^5	10,700	185.9	[43]
$(HTPP)_2MnBr_4$	Glass	$MnBr_4^{2-}$	519 Green	1.9×10^5	8,600	185	[44]
$(C_{20}H_{20}P)_2SbCl_5$	Glass	$SbCl_5^{2-}$	650 Orange	3.58×10^3	12,535	3.1×10^3	[42]
$(DMAC\text{-}TPP)_2ZnBr_4$	Amorphous	$DMAC\text{-}TPP^+$	518 Green	12.5	27,000	9.00	This work

varying spatial frequencies. To the best of our knowledge, this is the first flexible, fabric-based scintillator achieving spatial resolution comparable to conventional composite scintillators, highlighting its strong potential for wearable and conformal X-ray imaging applications. It is worth emphasizing that the amorphous nature of our material plays a crucial role in enabling the fabrication of flexible and wearable scintillating fabrics, representing a key advancement achieved in this work. To highlight the advantages of 0D $(DMAC\text{-}TPP)_2ZnBr_4$, we compare its scintillation performance to various previously developed 0D OMHH scintillators (Table 1). In general, amorphous systems tend to exhibit lower light yield than crystalline materials due to structural disorder and increased non-radiative pathways, and materials with organic-cation-based emissions exhibit much shorter decay lifetimes than those with metal-halide-centered emissions. With effective molecular sensitization and the intrinsically high PLQY of our rationally designed $DMAC\text{-}TPP^+$ cation, our amorphous $(DMAC\text{-}TPP)_2ZnBr_4$ system is able to deliver both high light yield and fast response.

Conclusion

In summary, we have demonstrated a rational molecular design strategy for developing high-performance X-ray scintillators by employing fluorescent cations to construct fully amorphous 0D OMHH films. This approach combines the strong X-ray absorption capability of metal halides with the efficient, short decay lifetime light emission of organic cations, enabling precise tailoring of optical properties for scintillation applications. The solution-processed amorphous 0D $(DMAC\text{-}TPP)_2ZnBr_4$ films exhibit bright green emission, a high photoluminescence quantum yield (~85%), and exceptional scintillation performance, including a high absolute light yield of ~27,000 photons MeV^{-1}, a short RL decay lifetime (~8.00 ns), an excellent dose linearity, and a low detection limit of ~9.00 nGy_{air} s^{-1}. These values rank among the best reported to date for 0D OMHH scintillators and represent the highest absolute light yield achieved for OMHH systems with nanosecond-scale decay lifetimes. The amorphous nature of the films, achieved via facile solution processing and mild thermal annealing, offers excellent low-cost processability and enables the fabrication of flexible, large-area devices, including wearable scintillating fabrics for X-ray imaging. This work not only highlights the promise of OMHHs as scalable scintillation platforms but also lays the groundwork for the development of flexible, cost-effective, and high-efficiency scintillators for applications in medical imaging, security screening, and radiation detection.

Supporting Information

The authors have cited additional references within the Supporting Information.[4,55–58]

Acknowledgements

The authors thank the support from the National Science Foundation (DMR-2204466 and ITE-2331357). This work was also partly funded by the EU Horizon grant 101112053. A portion of this research used resources provided by the X-ray Crystallography Center (FSU075000XRAY) and the Materials Characterization Laboratory (FSU075000MAC) at the FSU Department of Chemistry and Biochemistry.

Conflict of Interests

The Florida State University Research Foundation, Inc. has filed a provisional patent application based on this work with the United States Patent and Trademark Office (U.S. Provisional Patent No. 63/840253). Tarannuma Ferdous Manny and Biwu Ma are listed as inventors.

Data Availability Statement

The data that support the findings of this study are available in the Supporting Information of this article.

Keywords: Amorphous films • Molecular sensitization • Organic metal halide hybrids • Scintillators • X-ray detection

[1] L.-J. Xu, X. Lin, Q. He, M. Worku, B. Ma, *Nat. Commun.* **2020**, *11*, 4329, https://doi.org/10.1038/s41467-020-18119-y.

[2] A. Jana, S. Cho, S. A. Patil, A. Meena, Y. Jo, V. G. Sree, Y. Park, H. Kim, H. Im, R. A. Taylor, *Mater. Today* **2022**, *55*, 110–136, https://doi.org/10.1016/j.mattod.2022.04.009.

[3] T. B. Shonde, M. Chaaban, H. Liu, O. J. Olasupo, A. Ben-Akacha, F. G. Gonzalez, K. Julevich, X. Lin, J. R. V. Winfred, L. M. Stand, M. Zhuravleva, B. Ma, *Adv. Mater.* **2023**, *35*, 2301612, https://doi.org/10.1002/adma.202301612.

[4] T. F. Manny, T. B. Shonde, H. Liu, M. S. Islam, O. J. Olasupo, J. Viera, S. Moslemi, M. Khizr, C. Chung, J. R. V. Winfred, L. M. Stand, E. F. Hilinski, J. Schlenoff, B. Ma, *Adv. Funct. Mater.* **2025**, *35*, 2413755, https://doi.org/10.1002/adfm.202413755.

[5] X. Ou, X. Chen, X. Xu, L. Xie, X. Chen, Z. Hong, H. Bai, X. Liu, Q. Chen, L. Li, H. Yang, *Research* **2021**, *2021*, 9892152, https://doi.org/10.34133/2021/9892152.

[6] P. Lecoq, *Nucl. Instrum. Methods Phys. Res. Sect. A* **2016**, *809*, 130–139, https://doi.org/10.1016/j.nima.2015.08.041.

[7] T. B. Shonde, A. Mondal, H. Liu, M. Chaaban, A. Ben-Akacha, S. Lee, E. S. Knorr, B. Ma, *ACS Mater. Lett.* **2022**, *4*, 271–276, https://doi.org/10.1021/acsmaterialslett.1c00725.

[8] Q. He, C. Zhou, L. Xu, S. Lee, X. Lin, J. Neu, M. Worku, M. Chaaban, B. Ma, *ACS Mater. Lett.* **2020**, *2*, 633–638, https://doi.org/10.1021/acsmaterialslett.0c00133.

[9] Q. Chen, J. Wu, X. Ou, B. Huang, J. Almutlaq, A. A. Zhumekenov, X. Guan, S. Han, L. Liang, Z. Yi, *Nature* **2018**, *561*, 88–93, https://doi.org/10.1038/s41586-018-0451-1.

[10] Y. C. Kim, K. H. Kim, D.-Y. Son, D.-N. Jeong, J.-Y. Seo, Y. S. Choi, I. T. Han, S. Y. Lee, N.-G. Park, *Nature* **2017**, *550*, 87–91, https://doi.org/10.1038/nature24032.

[11] W. Shao, T. He, J.-X. Wang, Y. Zhou, P. Yuan, W. Wu, Z. Zhang, O. M. Bakr, H. Liang, O. F. Mohammed, *ACS Energy Lett.* **2023**, *8*, 2505–2512, https://doi.org/10.1021/acsenergylett.3c00784.

[12] M. Zhang, X. Wang, B. Yang, J. Zhu, G. Niu, H. Wu, L. Yin, X. Du, M. Niu, Y. Ge, *Adv. Funct. Mater.* **2021**, *31*, 2007921, https://doi.org/10.1002/adfm.202007921.

[13] Y. Liu, C. Gao, D. Li, X. Zhang, J. Zhu, M. Wu, W. Liu, T. Shi, X. He, J. Wang, *Nat. Commun.* **2024**, *15*, 1588, https://doi.org/10.1038/s41467-024-45871-2.

[14] S. Gupta, S. Sarisozen, S. Kumar Khuntia, F. Lang, P. Mahadevan, S. Bhattacharyya, *Adv. Funct. Mater.* **2025**, e14126, https://doi.org/10.1002/adfm.202514126.

[15] X. Du, S. Zhao, L. Wang, H. Wu, F. Ye, K.-H. Xue, S. Peng, J. Xia, Z. Sang, D. Zhang, *Nat. Photonics* **2024**, *18*, 162–169, https://doi.org/10.1038/s41566-023-01358-y.

[16] C. Dujardin, E. Auffray, E. Bourret-Courchesne, P. Dorenbos, P. Lecoq, M. Nikl, A. Vasil'Ev, A. Yoshikawa, R.-Y. Zhu, *IEEE Trans. Nucl. Sci.* **2018**, *65*, 1977–1997, https://doi.org/10.1109/TNS.2018.2840160.

[17] S. K. Gupta, Y. Mao, *Front. Optoelectron.* **2020**, *13*, 156–187, https://doi.org/10.1007/s12200-020-1003-5.

[18] S. Zhao, Z. Jia, Y. Huang, Q. Qian, Q. Lin, Z. Zang, *Adv. Funct. Mater.* **2023**, *33*, 2305858, https://doi.org/10.1002/adfm.202305858.

[19] T. Yanagida, *Proc. Jpn. Acad. Ser. B* **2018**, *94*, 75–97, https://doi.org/10.2183/pjab.94.007.

[20] A. Luo, J. Zhang, D. Xiao, G. Xie, X. Xu, Q. Zhao, C. Sun, Y. Li, Z. Zhang, P. Li, *Nat. Commun.* **2024**, *15*, 8181, https://doi.org/10.1038/s41467-024-51482-8.

[21] H. Zhang, Y. Tan, S. Gong, *Chem. Eur. J.* **2025**, *31*, e202404452.

[22] M. Koshimizu, *Jpn. J. Appl. Phys.* **2023**, *62*, 010503, https://doi.org/10.35848/1347-4065/ac94fe.

[23] Q. Q. Jia, G. Teri, Q. F. Zhou, J. Q. Luo, H. F. Ni, P. Z. Huang, P. G. Liu, L. Pan, C. F. Wang, Z. Liu, *Angew. Chem. Int. Ed.* **2025**, *64*, e202514669, https://doi.org/10.1002/anie.202514669.

[24] T. Jin, Z. Liu, J. Luo, J.-H. Yuan, H. Wang, Z. Xie, W. Pan, H. Wu, K.-H. Xue, L. Liu, *Nat. Commun.* **2023**, *14*, 2808, https://doi.org/10.1038/s41467-023-38545-y.

[25] Z. Xiang, J. Chen, T. Huang, F. Shen, X. Chen, J. Wang, Y. Wei, W. Wang, H. Cao, X. Ouyang, *Adv. Mater.* **2025**, *37*, 2414784, https://doi.org/10.1002/adma.202414784.

[26] M. Li, Z. Xia, *Chem. Soc. Rev.* **2021**, *50*, 2626–2662, https://doi.org/10.1039/D0CS00779J.

[27] W. Shao, G. Zhu, X. Wang, Z. Zhang, H. Lv, W. Deng, X. Zhang, H. Liang, *ACS Appl. Mater. Interfaces* **2023**, *15*, 932–941, https://doi.org/10.1021/acsami.2c16554.

[28] T. Xu, Y. Li, M. Nikl, R. Kucerkova, Z. Zhou, J. Chen, Y.-Y. Sun, G. Niu, J. Tang, Q. Wang, *ACS Appl. Mater. Interfaces* **2022**, *14*, 14157–14164, https://doi.org/10.1021/acsami.1c23839.

[29] Z.-Z. Zhang, J.-H. Wei, J.-B. Luo, X.-D. Wang, Z.-L. He, D.-B. Kuang, *ACS Appl. Mater. Interfaces* **2022**, *14*, 47913–47921, https://doi.org/10.1021/acsami.2c14582.

[30] N. Lin, X. Wang, H.-Y. Zhang, K.-Q. Sun, L. Xiao, X.-Y. Zhang, C.-Y. Yue, L. Han, Z.-W. Chen, X.-W. Lei, *ACS Appl. Mater. Interfaces* **2024**, *16*, 41165–41175, https://doi.org/10.1021/acsami.4c07376.

[31] Z. Z. Zhang, Z. L. He, J. B. Luo, J. H. Wei, X. X. Guo, J. H. Chen, D. B. Kuang, *Adv. Opt. Mater.* **2024**, *12*, 2302434, https://doi.org/10.1002/adom.202302434.

[32] T. He, Y. Zhou, X. Wang, J. Yin, L. Gutiérrez-Arzaluz, J.-X. Wang, Y. Zhang, O. M. Bakr, O. F. Mohammed, *ACS Energy Lett.* **2022**, *7*, 2753–2760, https://doi.org/10.1021/acsenergylett.2c01484.

[33] J. H. Han, T. Samanta, Y. M. Park, H. J. Kim, N. S. Manikanta Viswanath, H. W. Kim, B. K. Cha, S. B. Cho, W. B. Im, *ACS Energy Lett.* **2023**, *8*, 545–552, https://doi.org/10.1021/acsenergylett.2c02469.

[34] T. He, Y. Zhou, P. Yuan, J. Yin, L. Gutierrez-Arzaluz, S. Chen, J.-X. Wang, S. Thomas, H. N. Alshareef, O. M. Bakr, *ACS Energy Lett.* **2023**, *8*, 1362–1370, https://doi.org/10.1021/acsenergylett.3c00097.

[35] Z.-Z. Zhang, Z.-L. He, Q.-P. Peng, J.-H. Chen, B. Lan, D.-B. Kuang, *J. Mater. Chem. C* **2024**, *12*, 17411–17418, https://doi.org/10.1039/D4TC03459G.

[36] L. Zhou, J. F. Liao, D. B. Kuang, *Adv. Opt. Mater.* **2021**, *9*, 2100544, https://doi.org/10.1002/adom.202100544.

[37] J. Jin, K. Han, Y. Hu, Z. Xia, *Adv. Opt. Mater.* **2023**, *11*, 2300330, https://doi.org/10.1002/adom.202300330.

[38] S. B. Xiao, X. Zhang, X. Mao, H. J. Yang, Z. N. Chen, L. J. Xu, *Adv. Funct. Mater.* **2024**, *34*, 2404003, https://doi.org/10.1002/adfm.202404003.

[39] W. Lv, Y. Tang, C. Han, Z. Miao, C. Sun, L. Xu, G. Wu, Z. Liu, Y. Tao, R. Chen, *Inorg. Chem.* **2025**, *64*, 11032–11041, https://doi.org/10.1021/acs.inorgchem.5c01148.

[40] M. Zhou, H. Jiang, T. Hou, S. Hou, J. Li, X. Chen, C. Di, J. Xiao, H. Li, D. Ju, *Chem. Eng. J.* **2024**, *490*, 151823, https://doi.org/10.1016/j.cej.2024.151823.

[41] Q. Q. Jia, Z. X. Zhang, H. F. Ni, Q. Lin, G. Teri, P. G. Liu, J. Q. Luo, P. Z. Huang, Z. J. Wang, C. F. Wang, *Angew. Chem. Int. Ed.* **2025**, *64*, e202505163, https://doi.org/10.1002/anie.202505163.

[42] T. Feng, Z. a. Zhou, Y. n. An, L. Chen, Y. Fu, S. Zhou, N. Wang, J. Zheng, C. Sun, *ACS Nano* **2024**, *18*, 16715–16725, https://doi.org/10.1021/acsnano.4c01761.

[43] B. Li, K. Han, Y. Wang, Y. Sun, Z. Xia, Y. Xu, *Angew. Chem. Int. Ed.* **2025**, *64*, e202502440.

[44] J. B. Luo, J. H. Wei, Z. Z. Zhang, Z. L. He, D. B. Kuang, *Angew. Chem. Int. Ed.* **2023**, *62*, e202216504.
[45] L. Liu, H. Hu, W. Pan, H. Gao, J. Song, X. Feng, W. Qu, W. Wei, B. Yang, H. Wei, *Adv. Mater.* **2024**, *36*, 2311206, https://doi.org/10.1002/adma.202311206.
[46] Z. Z. Zhang, Z. L. He, J. B. Luo, J. H. Wei, X. X. Guo, J. H. Chen, D. B. Kuang, *Adv. Opt. Mater.* **2024**, *12*, 2302434, https://doi.org/10.1002/adom.202302434.
[47] B. Li, Y. Xu, X. Zhang, K. Han, J. Jin, Z. Xia, *Adv. Opt. Mater.* **2022**, *10*, 2102793, https://doi.org/10.1002/adom.202102793.
[48] B. Li, Y. Wang, Y. Xu, Z. Xia, *Adv. Mater.* **2025**, *37*, 2415483, https://doi.org/10.1002/adma.202415483.
[49] B. Li, Y. Sun, Y. Wang, J. Jin, K. Han, Y. Xu, Z. Xia, *Matter* **2025**, 102214.
[50] S. Chkoundali, F. Hlel, H. Khemekhem, *Appl. Phys. A* **2016**, *122*, 1066, https://doi.org/10.1007/s00339-016-0596-4.
[51] M. Taylor, R. Smith, F. Dossing, R. Franich, *Med. Phys.* **2012**, *39*, 1769–1778, https://doi.org/10.1118/1.3689810.
[52] M. Berger, J. Hubbell, S. Seltzer, J. Chang, J. Coursey, R. Sukumar, D. Zucker, K. Olsen, NIST, PML, Radiation Physics Division.
[53] H. Wei, Y. Fang, P. Mulligan, W. Chuirazzi, H.-H. Fang, C. Wang, B. R. Ecker, Y. Gao, M. A. Loi, L. Cao, *Nat. Photonics* **2016**, *10*, 333–339, https://doi.org/10.1038/nphoton.2016.41.
[54] D.-Y. Li, Y.-B. Shang, Q. Liu, H.-W. Zhang, X.-Y. Zhang, C.-Y. Yue, X.-W. Lei, *Mater. Horiz.* **2023**, *10*, 5004–5015, https://doi.org/10.1039/D3MH00536D.
[55] X. Wang, H. Shi, H. Ma, W. Ye, L. Song, J. Zan, X. Yao, X. Ou, G. Yang, Z. Zhao, *Nat. Photonics* **2021**, *15*, 187–192, https://doi.org/10.1038/s41566-020-00744-0.
[56] J. T. De Haas, P. Dorenbos, *IEEE Trans. Nucl. Sci.* **2008**, *55*, 1086–1092, https://doi.org/10.1109/TNS.2008.922819.
[57] A. Pron, P. Gawrys, M. Zagorska, D. Djurado, R. Demadrille, *Chem. Soc. Rev.* **2010**, *39*, 2577, https://doi.org/10.1039/b907999h.
[58] A. Shafiee, M. M. Salleh, M. Yahaya, *Sains Malaysiana* **2011**, *40*, 173–176.

Manuscript received: November 14, 2025
Revised manuscript received: December 05, 2025
Manuscript accepted: December 08, 2025
Version of record online: December 16, 2025